Materials and Design 37 (2012) 152–160

Contents lists available at SciVerse ScienceDirect

Materials and Design

journal homepage: www.elsevier.com/locate/matdes

Formation mechanism and characterization of nanostructured Ti6Al4V alloy prepared by mechanical alloying

A. Mahboubi Soufiani *, F. Karimzadeh, M.H. Enayati

Department of Materials Engineering, Isfahan University of Technology, Isfahan 84156-83111, Iran

ARTICLE INFO

Article history:
Received 11 November 2011
Accepted 28 December 2011
Available online 11 January 2012

Keywords:
A. Nanomaterials
B. Particulates and powders
C. Mechanical alloying

ABSTRACT

In recent years, researches on properties of nanocrystalline materials in comparison with coarse-grained materials have attracted a great deal of attention. The present investigation has been based on production of nanocrystalline Ti6Al4V powder from elemental powders by means of high energy mechanical milling. In this regard, Ti, Al and V powders were milled for up to 90 h and heat treated at different temperatures. The structural and morphological changes of powders were investigated by X-ray diffraction (XRD), scanning electron microscopy (SEM), differential thermal analysis (DTA) and microhardness measurements. The results demonstrated that Ti(Al) and Ti(Al, V) solid solutions with grain size of 95 and 20 nm respectively form during mechanical alloying. In addition, an amorphous structure was obtained at longer milling times. The crystallization of amorphous phase upon annealing led to the formation of nanostructured Ti6Al4V phase with a grain size of 20–50 nm. The as-milled Ti6Al4V powder with amorphous structure exhibited a high microhardness of ~720 Hv. Upon crystallization the hardness value reduced to ~630 Hv which is higher than those reported for Ti6Al4V alloys processed by conventional routes.

1. Introduction

Titanium and titanium alloys have been widely employed in industrial and biomedical applications because of their low modulus of elasticity, relatively low density, high specific strength, good biocompatibility and corrosion resistance [1,2]. Among these, Ti6Al4V (Ti–6 wt%Al–4 wt%V) has been the most promising and highly used $\alpha + \beta$ titanium alloy [3].

Every processing method has its associated advantages and disadvantages. It has been established that the high purity aeronautical (and for other applications as well) grade of titanium alloys are produced through conventional casting and thermomechanical processing route [4,5]. In order to overcome the shortcomings of conventional production methods [6,7], powder metallurgy and solid state production processes have attracted a great amount of investment. It is important to mention that titanium being superplastic in nature can be processed to near net shape by isothermal forging.

In recent years, nanostructured materials have gained considerable attention due to their improved properties in comparison with conventional micro sized structured materials [8]. In this regard, a wide range of investigations have been dedicated to alterations in mechanical, thermal, magnetic and diffusion characteristics of nanocrystalline materials [9,10]. Due to many noteworthy advantages, fabrication of nanostructured metals such as Ni, Fe, Al and Zn has already been taken into consideration [11–13]. In addition, with the aim of enhancing the strength and tribological properties of titanium and its alloys, a number of researches have contributed to the preparation of nanostructured Ti alloys [14,15]. In our previous investigation [16], the improvements in the physical and mechanical properties of nanostructured Ti6Al4V alloy powder fabricated from residual scraps was studied.

One of the most cost-effective methods that has proven to be capable of producing powders with nano-sized structure is mechanical alloying (MA) [14]. This process has been utilized in fabrication of different products such as nanostructured alloys, intermetallic compounds and metal matrix composites [17–19]. Furthermore, there is limited information reported on the fabrication of nanostructured ternary titanium alloy systems such as, Ti–Al–V, Ti–Al–Si and Ti–Al–Mg, by MA [20–22].

The current study, therefore, is set up with the aim of producing nanostructured Ti6Al4V alloy from elemental powders by means of mechanical alloying (MA). The present report focuses mainly on characterization and some preliminary measurements of the thermal, mechanical and physical properties of the nanostructured Ti6Al4V powders fabricated.

2. Experimental procedure

Elemental powders of Ti, Al and V with average particle size of 400 μm, 70 μm and 20 μm, purity of 99.99, 99.97 and 99.99 wt%

* Corresponding author. Tel.: +98 9133142314; fax: +98 3113912751.
E-mail address: a.soofiani@ma.iut.ac.ir (A. Mahboubi Soufiani).

0261-3069/$ - see front matter © 2012 Elsevier Ltd. All rights reserved.
doi:10.1016/j.matdes.2011.12.044

and irregular, oblong and edged particle shape, respectively, were mixed in the desired composition (Ti–6 wt%Al–4 wt%V). The SEM micrographs of as-received powder are presented in Fig. 1.

Mechanical milling was applied under a protective atmosphere of Ar (99.998% pure) in a planetary ball mill. Milling parameters are given in Table 1.

Small quantities of <1 g of powder were withdrawn from milled materials at selected intervals (every 5 h up to 90 h). Powder samples were placed in steel tubes with sealed ends and were subjected to heat treatment in a tube furnace under an Ar atmosphere at different temperatures (550 °C, 650 °C, 710 °C, 750 °C and 900 °C) and time periods (30, 45 and 60 min). The structure and phase composition of mechanically milled and heat treated powders was characterized by means of X-ray diffraction (Philips X'PERT MPD) using filtered Cu Kα radiation (λ = 0.1542 nm).

The average crystallite size and internal strain in the milled samples were calculated from the XRD peak broadening using the Williamson–Hall equation [23]:

$$\beta\cos\theta = \frac{K\lambda}{D} + 2A\sqrt{(\varepsilon)^2}\sin\theta \quad (1)$$

where θ is the Bragg diffraction angle, D the average crystallite size, ε the average internal strain, λ the wave length of the radiation used (0.15406 nm), β the diffraction peak width at half maximum intensity, K the Scherrer constant (0.9) and A is the coefficient which depends on the distribution of strain; it is near to unity for dislocations. In the Williamson–Hall method, both of the broadening contributions, due to the strain and the crystallite size, are taken into account.

The morphologies and particle size of milled powders were determined utilizing a scanning electron microscope (Philips XL30) and in order to evaluate thermal behavior and phase evaluation of milled powder, differential thermal analysis (DTA) with a heating rate of 10 °C/min was utilized.

Table 1
Milling parameters.

Ball mill machine	Planetary
Rotation speed of vial (rpm)	500
Vial material	Hardened Cr steel
Vial capacity (ml)	120
Ball material	Hardened carbon steel
Diameter of balls (mm)	20
Number of balls	5
Ball to powder weight ratio	10:1
Total powder mass (g)	16.3

The microhardness test was carried out at a load of 37.64 g and dwell time of 5 s. Five indentations were made on each sample to obtain an average value of microhardness. The microhardness measurement was carried out on the cross-section of powder particles. The samples were prepared by mounting a small amount of powder in a carbon-based conductive resin followed by conventional grinding and polishing methods.

3. Results and discussion

3.1. Phase evaluation during milling

Different phase transformations in Ti–6 wt%Al–4 wt%V powder mixture during mechanical milling process were studied by the X-ray diffraction method.

Fig. 2 presents the XRD patterns of Ti6Al4V powder before and after 5, 10, 20, 40, 60, 80 and 90 h of milling. As can be seen, after 5 h of milling Ti peaks are broadened and Al peaks have

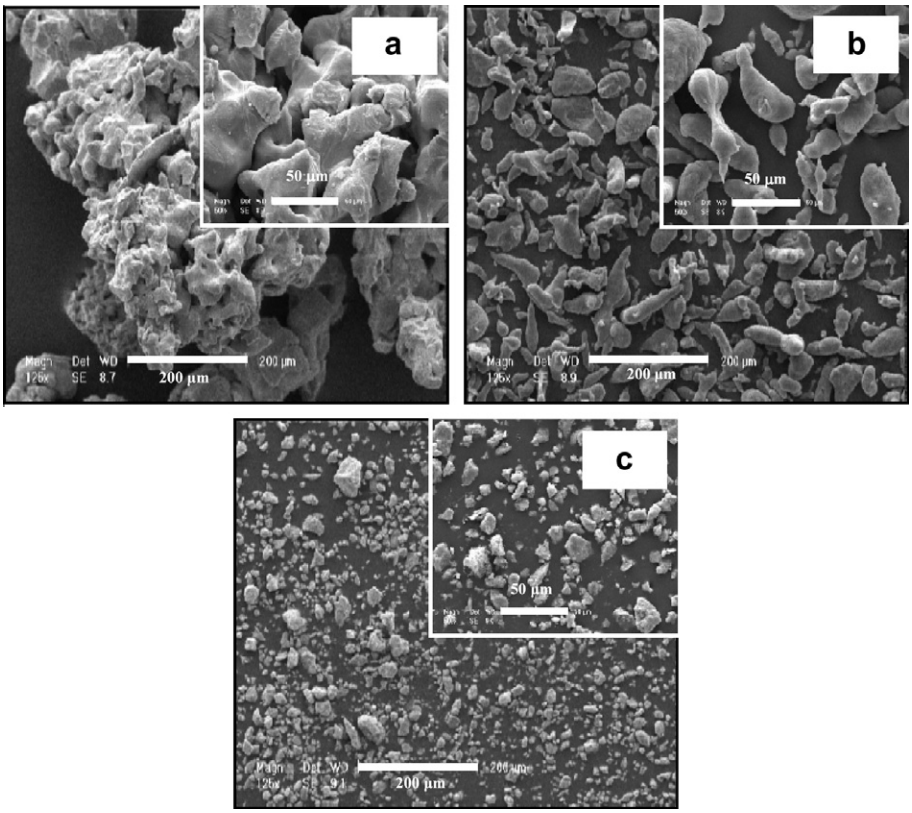

Fig. 1. SEM micrographs of the morphology of as-received (a) Ti, (b) Al and (c) V powders.

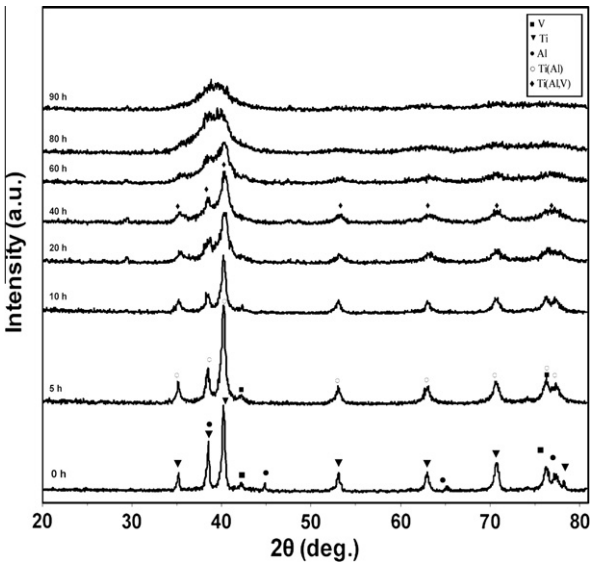

Fig. 2. XRD patterns of Ti–6 wt%Al–4 wt%V powder samples as-received and after 5, 10, 20, 40, 60, 80 and 90 h of mechanical alloying.

disappeared. This broadening trend of Ti main peaks continues toward 10 h.

Fig. 3 indicates a Ti (101) peak shift after 10 h of milling at higher magnitude. This Ti peak's gradual angular shift to higher angles is mainly attributed to the formation of Ti(Al) solid solution and negligibly to lattice parameter reduction as a result of grain compression. Considering that the Al melting point (660 °C) and atomic radius (1.43 Å) are smaller than for Ti (1.47 Å), due to cold welding of particles and formation of a lamella structure in the first stages of mechanical alloying process, Al with a higher diffusion coefficient can readily dissolve in the Ti, forming a homogenous Ti(Al) solid solution. As a result, the Ti lattice parameter and subsequently the planes distance (d = 0.119 nm) reduced, followed by a diffraction angle increase (2θ = 40.3°) in accordance to the Brag law [24]. Formation of hcp Ti(Al) solid solution prior to the formation of an amorphous phase has also been reported in other investigations [25–27].

The extent of Ti peak replacement is in direct relation to the percentage of dissolved Al [28]. Due to low Al to Ti ratio (10 at%Al–86 at%Ti) in the current study the change in Ti lattice parameters and overall lattice distortion that resulted from Al

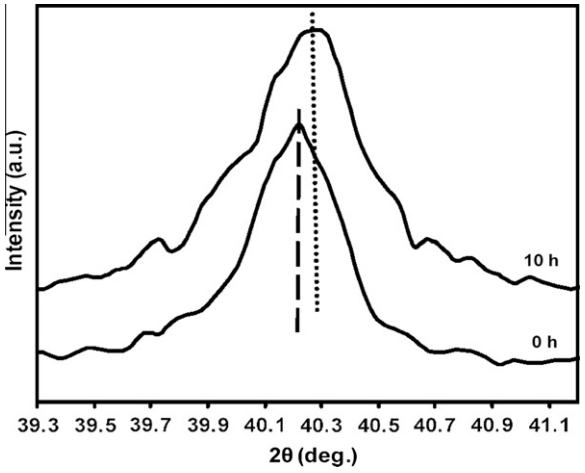

Fig. 3. Ti (101) peak shift after 10 h milling.

diffusion was negligible (Fig. 3). The lattice parameters, a = 0.293 nm and c = 0.466 nm, were measured for hcp Ti(Al) solid solution after 10 h of mechanical milling, which is truly in agreement with the data cited by Fadeeva et al. [29].

The mechanical alloying procedure, as a non-equilibrium process, is capable of changing the solubility limitations of different elements [14]. According to the Ti–Al equilibrium phase diagram [30], the maximum solubility of Al in Ti at ambient temperature is about 11 at%. Moreover, it has been reported that formation of Ti_3Al intermetallic during mechanical alloying in Ti–Al systems with Al content less than 6.5 at% is improbable [31].

As illustrated in the XRD patterns in Fig. 2, up to 20 h there still exists pure vanadium. Given that it has a smaller atomic radius than titanium (V_r = 1.35 A°, Ti_r = 1.47 A°) and also a lower diffusion coefficient than aluminum (T_m(V) = 1890 °C), formation of the solid solution containing V takes longer milling periods. However, the Ti–V equilibrium phase diagram indicates high solubility of V in Ti at ambient temperature.

With continuing milling up to 40 h, repeated cold welding and fracturing and increased density of crystalline defects and dislocations resulted in successful diffusion of V and formation of Ti(Al, V) solid solution. Dutkiewicz et al. [32] have proven that β stabilizing elements require longer mechanical alloying hours in order to diffuse in Ti lattice. Furthermore, in order to facilitate V diffusion into Ti lattice and form solid solution, after initial mixing of the powders, Jakubowicz et al. [33] exposed the powder sample to elevated temperatures.

The actual dominant trend during milling for more than 5 h was Ti peak intensity reduction and broadening. These changes are the results of grain refinement and internal strain elevation caused by work hardening during mechanical milling. The increase in dislocation density, stacking fault energy, local strain around dislocation and formation of low angle boundaries due to recovery and dislocation redistribution has led to peak broadening in XRD patterns [34]. The crystallite sizes measured by the Williamson–Hall method after 10 and 40 h of milling for Ti(Al) and Ti(Al, V) phases were 95 and 20 nm, respectively (Table 2).

Mechanical alloying for 60 h resulted in excessive Ti(Al, V) phase peak broadening and this solid solution appears to have partially transformed into an amorphous phase. As Zhao et al. have claimed [21], with an increase in Al content of Ti(Al) solid solution the tendency towards forming an amorphous phase in shorter milling times increases. Considering the XRD patterns, after 90 h of milling the obtained structure becomes generally amorphous. In this condition, the amorphous phase peak position happens at about 2θ = 39.57°. According to the Ehrenfest equation (2), the mean nearest neighbor atom distance in the amorphous phase (r) was estimated to be about 0.273 nm.

$$2r\sin\theta = 1.2\lambda \tag{2}$$

where θ is peak position and λ is X-ray wave length [35].

3.2. Structural changes during isothermal annealing

In order to evaluate the thermal behavior, the 60 h mechanically milled sample was annealed for 30, 45 and 60 min at 650 °C.

Table 2
The crystallite size and internal strain of Ti–6 wt%Al–4 wt%V powders after 10 and 40 h of mechanical milling.

Milling time (h)	Crystallite size (nm)	Internal strain (%)
10 Ti(Al)	95	0.31
40 Ti(Al, V)	20	0.76

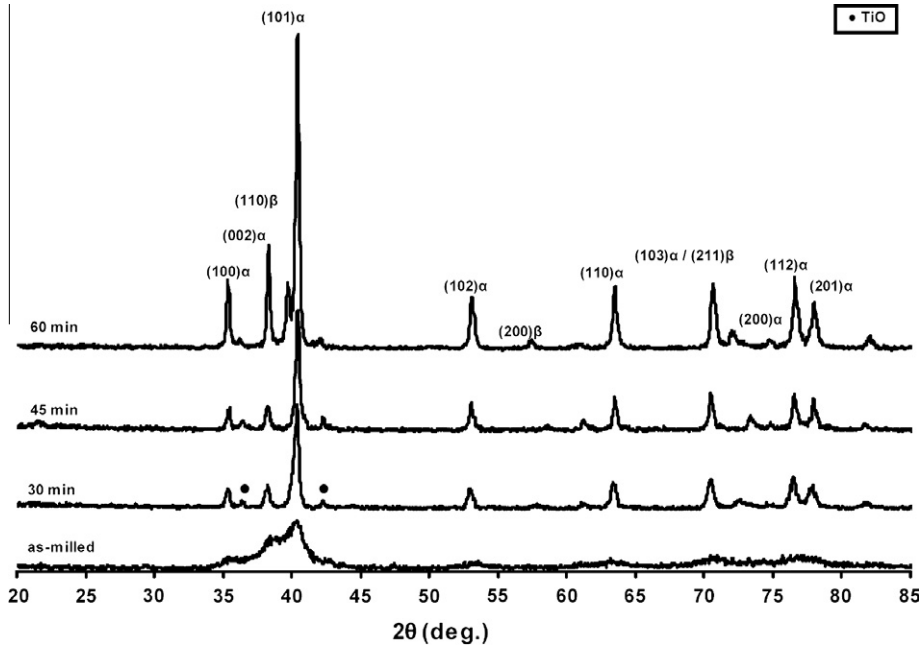

Fig. 4. XRD patterns of Ti(Al, V) powder as-milled for 60 h and after subsequent annealing for 30, 45 and 60 min at 650 °C.

Fig. 4 illustrates the XRD patterns of Ti(Al, V) solid solution samples before and after annealing. Considering the high oxidation tendency of Ti in the presence of V and inevitable oxygen infiltration in the furnace, the annealing temperature was fixed at 650 °C in order to prevent excessive oxidation [36].

As can be seen, after 30 min of annealing the amorphous phase experienced general crystallization and nearly all the Ti6Al4V main peaks became clearly detectable. Due to the short annealing time and cooling samples in air, the crystalline phase formed during crystallization did not undergo excessive grain growth. The crystallite size calculated applying the Williamson–Hall method for Ti6Al4V phase after annealing for 30 min was estimated to be ~50 nm. The presence of a negligible amount of TiO after 30 min of annealing is a sign of undesirable oxidation that has also been reported by Sun et al. [37].

Samples annealed for 45 min showed the same behavior as 30 min samples, with a slight increase in peak intensity. The measured crystallite size for this sample (~60 nm) featured very little grain growth in comparison with that of the 30 min sample. As can be seen in Fig. 4, Ti(Al, V) powder subjected to 650 °C for 60 min holds sharp Ti6Al4V peaks together with remarkable peaks width reduction. This phenomenon represents intense grain growth which was confirmed by the measured grain size of 90 nm. In addition, by annealing for 60 min, the β phase (bcc) nucleated (Fig. 4), while after 30 and 40 min only a single α phase (hcp) was present. This indicates that vanadium diffusion for formation of regions with high concentration of β stabilizer is a very slow process and therefore, significantly time-dependent [38]. In the XRD pattern of the 60 min annealed sample, β(110), β(200) and β(211) main peaks are observable.

Fig. 5I illustrates the XRD patterns of Ti–6 wt%Al–4 wt%V as-milled for 90 h and after heat treatment. As can be seen, after annealing at 750 °C for 1 h the amorphous structure has completely transformed into nanocrystalline Ti6Al4V alloy with a grain size of 45 nm. Considering the placement of Al and V atoms in Ti lattice after heat treatment, the α(101) peak has shifted from $2\theta = 40.2°$ to about $2\theta = 40.45°$ (Fig. 5II) and in this condition hcp lattice parameters were $a = 0.292$ nm and $c = 0.464$.

The amorphous powder obtained after 90 h of mechanical alloying was also subjected to DTA and in the graph provided (Fig. 6) two exothermic peaks at 550 °C and 710 °C were observed. In order to characterize these exothermic peaks, 90 h milled powder was heated at a rate of 10 °C/min up to 550 °C, 710 °C and 900 °C in furnace, followed by cooling in air and XRD patterns were provided (Fig. 7). After heating up to 550 °C, a considerable portion of the structure still consists of the amorphous phase; however, nucleation of the α phase has commenced as traces of α(101) peak appeared on the XRD pattern. By increasing the temperature to 710 °C, a general α phase crystallization can be regarded as the main feature, while further heating up to 900 °C has been accompanied by complete crystallization followed by grain growth.

3.3. Morphological and microstructural changes during milling

The morphology of the milled powders obtained at different stages of the MA process was observed by SEM, and is presented in Fig. 8. The micrographs featured in this figure are of different magnifications. Fig. 9 shows the backscattered electron images of the cross-section views of the milled particles.

As is known, cold welding and fracturing are the two essential processes involved in mechanical alloying; therefore, changes in morphology are the results of the following stages: micro-forging, fracturing, agglomeration and de-agglomeration [39]. As can be seen in Fig. 8a, after 10 h of milling, the developed powder particles are equiaxed and have a broad range of size with an average diameter of 230 μm. Moreover, large agglomerated clusters consisting of smaller particles are apparent in the micrograph of higher magnification. With further milling to 20 h, owing to collision of balls, particles have faced size reduction in comparison with 10 h milled powder (Fig. 8b). With respect to morphological changes after 40 h of milling (Fig. 8c), the powder particles are characterized by narrow particle size distribution and diversity of shapes, irregular and spherical, with about 20 μm in diameter. This behavior is associated with a fracture process being predominant at this stage, while, the resulting particles are clusters consisting of cold welded smal-

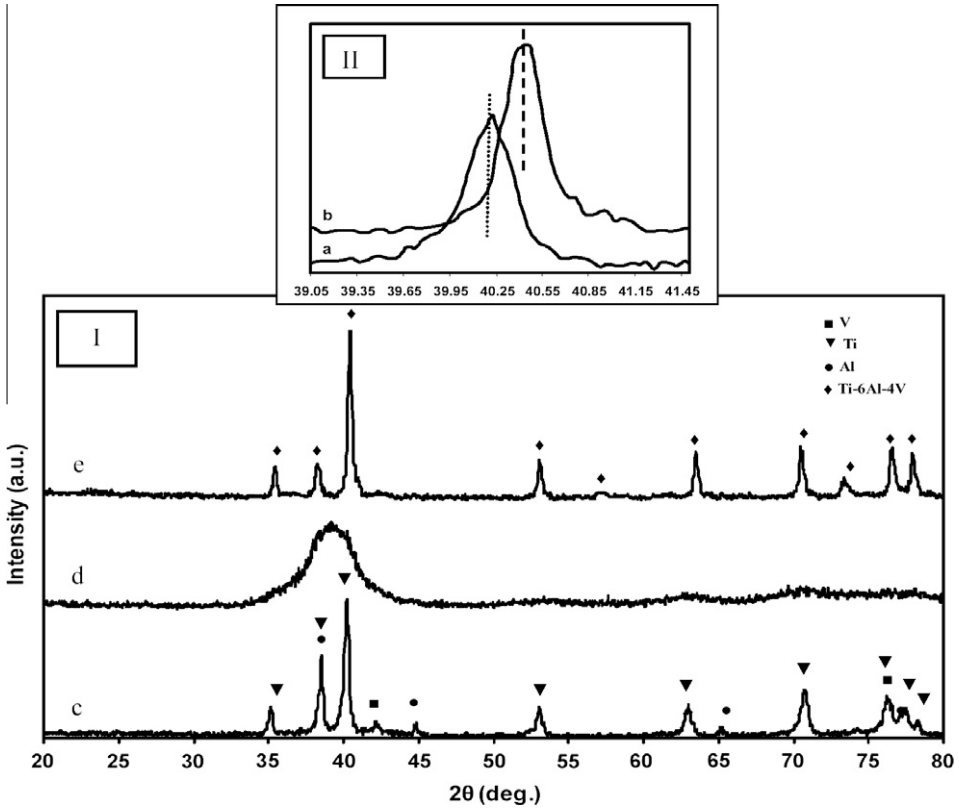

Fig. 5. (I) XRD patterns of Ti–6 wt%Al–4 wt%V powders (c) before, (d) after 80 h of MA and (e) after annealing for 1 h at 750 °C, (II) Ti α(1 0 1) peak shift after heat treatment (b) in comparison with initial powder (a).

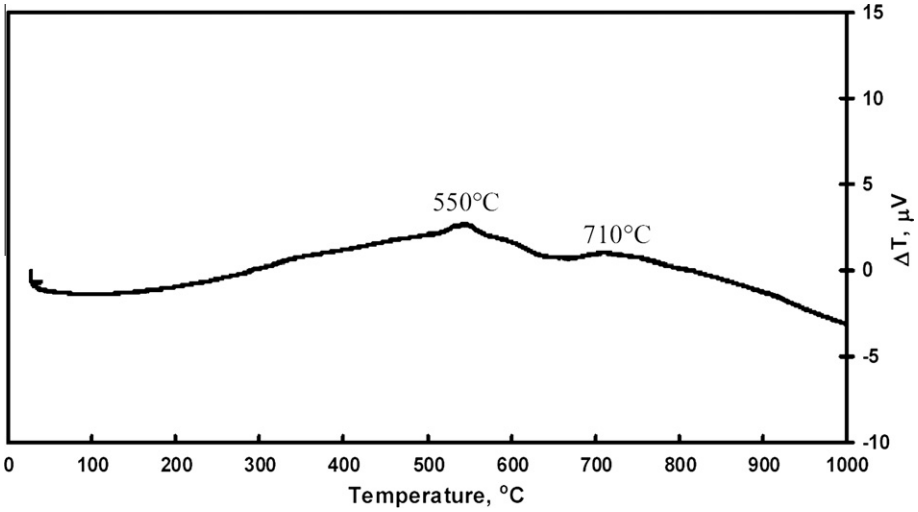

Fig. 6. DTA trace of the amorphous powder milled for 90 h.

ler particles. After 60 h of milling (Fig. 8d), both fracturing and cold welding processes are balanced and powder particles became more uniform and spherical compared to those of 40 h.

Fig. 8e indicates that milling for 90 h has been followed by significant particle refinement which led to formation of ~2 μm diameter particles. A higher magnification image reveals that these 2 μm particles are agglomerates of smaller particles of around 800 nm. At this final stage, fracturing has been the dominant process and the particles seem to have a uniform irregular shape. This brittle fracturing may be due to strain hardening induced by repeated welding, fracturing and re-welding of different constituent powders during the milling process and also formation of a homogeneous amorphous phase which has been shown in the XRD pattern of the 90 h milled sample.

Fig. 9 presents particle size changes with milling time. As it shows, in the 10–20 h milling stage (I), fracture has been predominant, whereas from 20 to 60 h (II) both cold welding and fracturing have been active. In the finishing stage of milling (III), particle refinement has occurred at a lower rate than that of the first stage.

A cross-sectional micrograph of 5 h milled powder sample is presented in Fig. 10a. In this beginning stage, different elemental powder particles are partially mixed and, due to the nature of

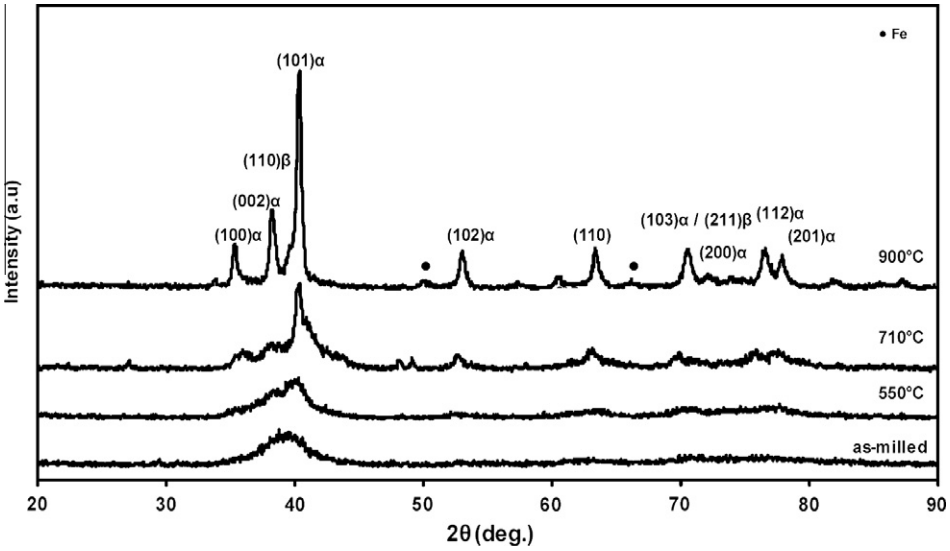

Fig. 7. XRD patterns of Ti–Al–V powder samples as-received and after MA for 90 h and after annealing in DTA up to 550 °C, 710 °C and 900 °C at the rate of 10 °C/min.

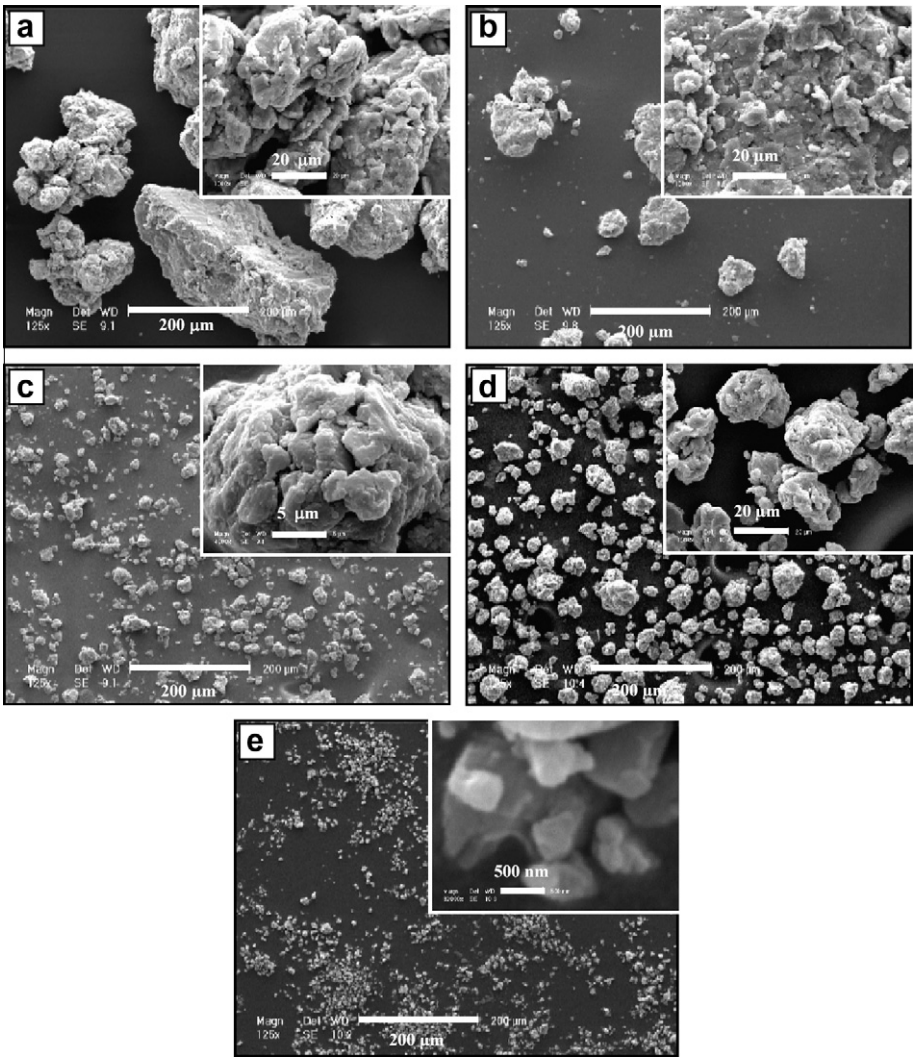

Fig. 8. SEM micrographs of powder mixture mechanically alloyed for (a) 10 h, (b) 20 h, (c) 40 h, (d) 60 h and (e) 90 h.

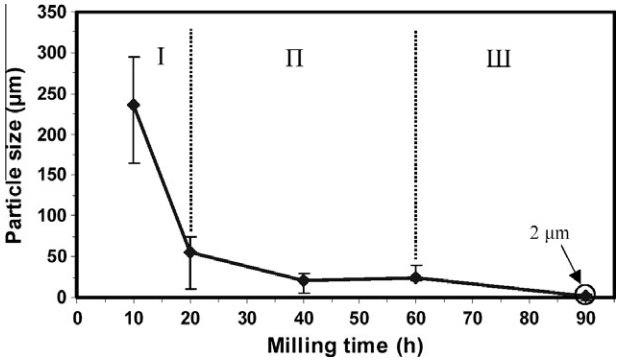

Fig. 9. Changes in powder particle size with milling time for Ti6Al4V.

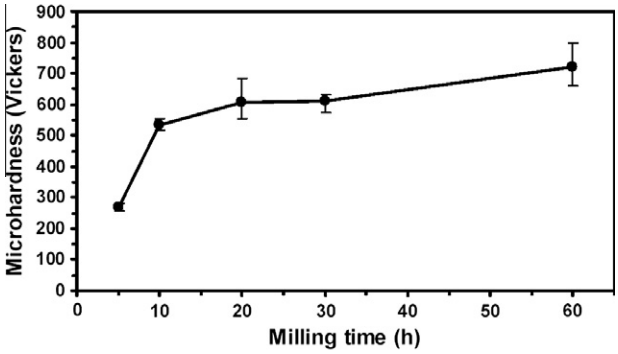

Fig. 11. Variation of microhardness value with milling time for Ti6Al4V powder mixture.

mechanical alloying, large blocks containing coarse layers have formed [14]. In the image of higher magnification, the presence of intact elemental powder particles along with a coarse layered structure is observable. This may be due to low plastic deformation in the early stages of MA. Formation of a coarse lamellae structure of initial powders in the first stages of mechanical alloying has also been reported in other literature [14,31].

After 10 h of milling (Fig. 10b), a finer layered structure has developed. Due to continuous cold welding and fracturing, coarse layers have been fractured and flattened by ball collision and subsequently fresh metal surfaces have been welded together. This process consequently results in layer thickness reduction (formation of fine layered structure) and inter-diffusion of elements across layers [14]. With further milling up to 40 h (Fig. 10c), the layers became hardly detectable. Reduction in layer thickness is followed by reduction of diffusion distance and accelerates the MA process [26]. Also, the XRD pattern of this sample indicates that Al and V have thoroughly diffused in Ti lattice and a partial amorphous structure has formed.

As can be seen in Fig. 10d, after 90 h of milling there exists no sign of a lamellae structure and a homogeneous amorphous phase is formed, and this is in complete agreement with the XRD results (Fig. 2).

3.4. Microhardness measurements

The changes in powder particles microhardness during milling is illustrated in Fig. 11. Due to intensive work hardening of ductile metallic particles in the first stages of mechanical milling, the hardness value increases significantly during 5–10 h of milling [14]. From 10 to 60 h of milling, as work hardening approaches its saturation and Ti(Al) and Ti(Al, V) solid solutions form, hardness increasing trend continues with a gentler slope. Particle size after 90 h of milling was ultra-fine so that the microhardness measurements were impossible.

The bar chart presented in Fig. 12 compares the average powder particle microhardness during milling and after heat treatment (60 h milled + 1 h at 650 °C). As can be seen, after annealing, Ti6Al4V alloy had the hardness value of ~630 Hv, which is smaller than that of 60 h as-milled powder (~720 Hv). This decrease in hardness is attributed to crystallization of the hard amorphous

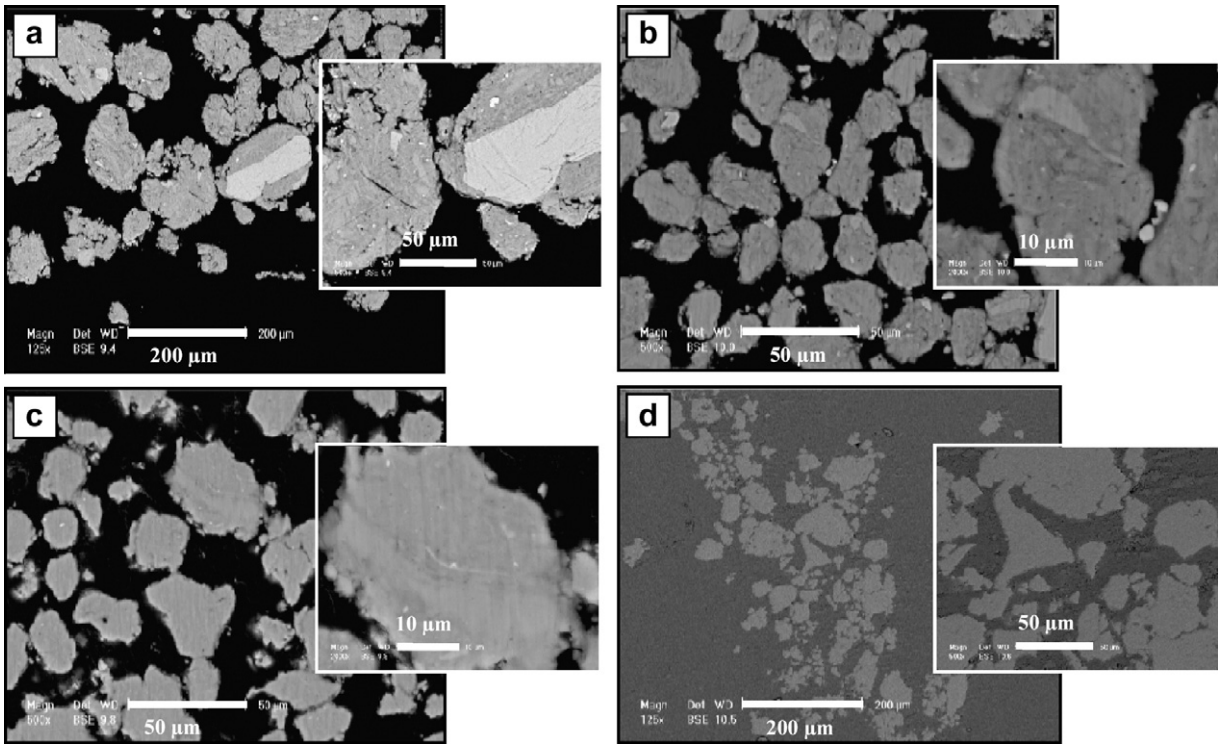

Fig. 10. SEM cross-section view of the milled Ti–6Al–4V powder mechanically milled for (a) 5 h, (b) 10 h, (c) 40 h and (d) 90 h.

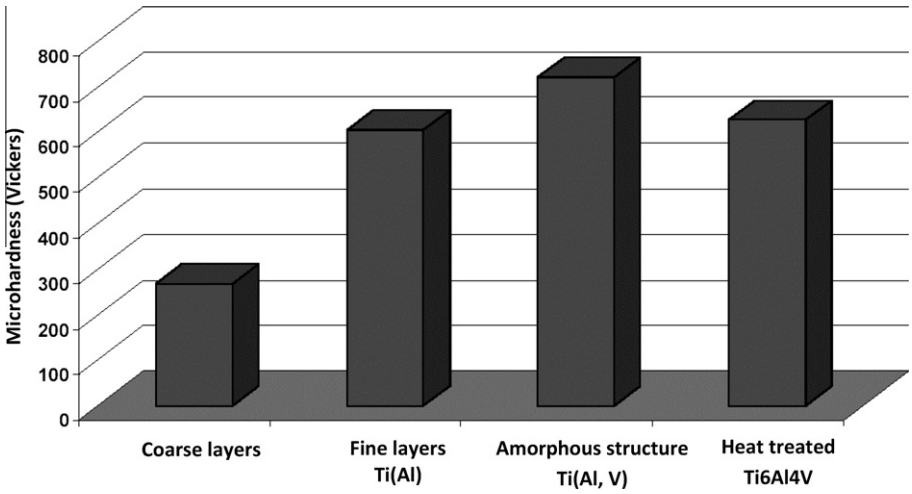

Fig. 12. Average microhardness value of the powder mixture at different stages of mechanical alloying and after annealing (60 h MA + 1 h at 650 °C).

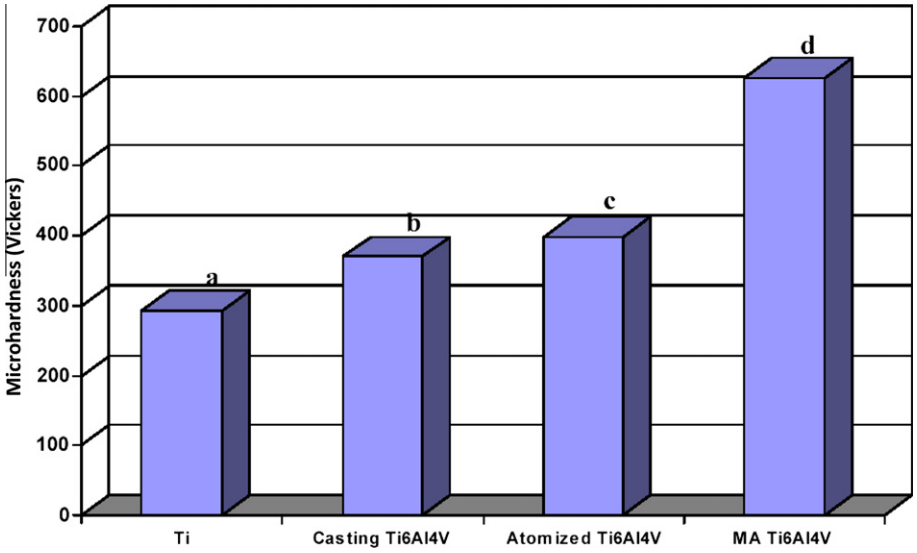

Fig. 13. Microhardness comparison between (a) titanium powder (99.98% pure) and (b) casting [40], (c) atomized [41] and mechanically alloyed Ti6Al4V alloy.

phase and formation of Ti6Al4V alloy containing α and β crystalline phases after annealing.

A comparison between the reported microhardness values of Ti6Al4V alloys produced via different processes can be seen in Fig. 13. The hardness of casted and heat treated [40], atomized [41] and mechanically milled residual scraps [42] of Ti6Al4V alloy were 370 Hv, 399 Hv and 536 Hv, respectively, which differ greatly from the nanostructured Ti6Al4V alloy formed by mechanical alloying (~630 Hv) in the current study.

4. Conclusions

Mechanical alloying of the Ti–Al–V system has been performed in order to examine the behavior of this ternary system for the formation of the Ti6Al4V nanostructured phase. The following conclusions were drawn:

(a) Mechanical alloying of Ti–Al–V system plus heat treatment led to the formation of nanostructured Ti6Al4V phase. The final crystallite size of the fabricated nanostructured alloy was measured to be 20–50 nm.

(b) Formation of nanostructured Ti6Al4V alloy consisted of different steps:

In first stages of mechanical alloying Al diffuses into Ti lattice and forms Ti(Al) pre-saturated solid solution. Then, at longer milling hours V tends to dissolve in this solid solution and Ti(Al, V) is obtained. Finally, with further milling the Ti(Al, V) phase becomes unstable and transforms to an amorphous phase.

(c) The amorphous phase crystallized upon annealing and led to the formation of Ti6Al4V α and β phases and a result a reduction in the microhardness value from 720 Hv to 630 Hv. The occurrence of microhardness reduction after annealing was mainly due to crystallization, achieving long-range ordered structure, grain growth and internal strain release. In comparison with other reported investigations, the microhardness of nanostructured Ti6Al4V alloy fabricated by means of MA is distinctively higher.

References

[1] Gonzalez JEG, Mirza Rosca JC. Study of the corrosion behavior of titanium and some of its alloys for biomedical and dental implant applications. J Electroanal Chem 1999;471:109–15.

[2] Mu Y, Kobayashi T, Sumtra M, Yamamoto A, Hanawa T. Metal ion release from titanium with active oxygen species generated by rat macrophages in vitro. J Biomed Mater Res 2000;49:283–7.

[3] McQuillan AD, McQuillan MK. Titanium. London: Butterworth; 1956.
[4] Zitnansky M, Caplovic L. The preparing of Ti6Al4V in laboratory conditions. J Mater Process Technol 2004;157:781–7.
[5] Syverud M, Okabe T, Hero H. Casting of Ti6Al4V alloy compared with pure Ti in an Ar-arc casting machine. Eur J Oral Sci 1995;103:327–30.
[6] Watanabe I, Woldu M, Watanabe K, Okabe T. Effect of casting method on castability of titanium and dental alloys. J Mater Sci 2000;11:547–53.
[7] Wang RR, Boyle AM. A simple method for inspection of porosity in titanium castings. J Prosthet Dent 1993;70:275–6.
[8] Morris DG. Mechanical behavior of nanostructured materials. Switzerland: Trans Tech Publications; 1998.
[9] Zhu KY, Vassel A, Brisset F, Lu K, Lu J. Nanostructure formation mechanism of a-titanium using SMAT. Acta Mater 2004;52:4101–10.
[10] Lauer S, Guan Z, Wolf H, Wichert Th. Structural investigations of nanocrystalline Ti–Al and Ni by PAC. Hyperfine Interact 1999;120/121:307–12.
[11] He J, Lavernia EJ. Development of nanocrystalline structure during cryomilling of Inconel 625. J Mater Res 2001;16:2724–31.
[12] Xun Y, Lavernia EJ, Mohamed FA. Processing and microstructural evolution of powder metallurgy Zn-22Pct Al eutectoid alloy containing nanoscale dispersion particles. Metall Mater Trans A 2004;35:573–83.
[13] Tellkamp VL, Dallek S, Lavernia EJ. Mechanical behavior and microstructure of thermally stable bulk nanostructured Al alloy. Metall Mater Trans A 2004;32:2535–43.
[14] Suryanarayana C. Mechanical alloying and milling. Prog Mater Sci 2001;46:1–184.
[15] Sun F, Froes FH. Synthesis and characterization of mechanical-alloyed Ti–*x*Mg alloys. J Alloys Compd 2002;340:220–5.
[16] Mahboubi Soufiani A, Enayati MH, Karimzadeh F. Fabrication and characterization of nanostructured Ti6Al4V powder from machining scraps. Adv Powder Technol 2010;21:336–40.
[17] Khodaei M, Enayati MH, Karimzadeh F. The structure and mechanical properties of Fe_3Al–30 vol.% Al_2O_3 nanocomposite. J Alloys Compd 2009;488:134–7.
[18] Mousavi T, Karimzadeh F, Abbasi MH. Mechanochemical assisted synthesis of NiTi intermetallic based nanocomposite reinforced by Al_2O_3. J Alloys Compd 2009;467:173–8.
[19] Rafie M, Enayati MH, Karimzadeh F. Characterization and formation mechanism of nanocrystalline $(Fe,Ti)_3Al$ intermetallic compound prepared by mechanical alloying. J Alloys Compd 2009;480:392–6.
[20] Caetano M, Trindade B. Synthesis of lightweight Ti–10Al–5Mg(wt%) alloy by mechanical alloying followed by compaction and sintering. J Mater Sci 2007;42:7684–9.
[21] Zhou JB, Rao KP. Structure and morphology evolution during mechanical alloying of Ti–Al–Si powder systems. J Alloys Compd 2004;384:125–30.
[22] Pirzada MDS, Patankar SN, Froes FH. Mechanochemical processing of nanocrystalline Ti6Al4V alloy. Moscow (ID): University of Idaho; 2004.
[23] Williamson GK, Hall WH. X-ray line broadening from field aluminum and wolfram. Acta Metal 1953;1:22–31.
[24] Liu W, Liu Y. Mechanical alloying and spark plasma sintering of the intermetallic compound $Ti_{50}Al_{50}$. J Alloys Compd 2007;440:154–7.
[25] Forouzanmehr N, Karimzadeh F, Enayati MH. Synthesis and characterization of $TiAl/Al_2O_3$ nanocomposite by mechanical alloying. J Alloys Compd 2009;478:257–9.
[26] Suryanarayana C, Chen G, Abdulbaset F, Froes FH. Structural evolution of mechanically alloyed Ti–Al alloys. Mater Sci Eng A 1992;158:93–101.
[27] Itsukaichi T, Masuyama K, Umemoto M, Okane I, Cabanas-Moreno JG. Mechanical alloying of Ti–Al powder mixture and their subsequent consolidation. J Mater Res 1993;8:1817–28.
[28] Zhou JB, Rao KP, Chung CY. Preparation of metastable precursors with different compositions of Ti–Al–Si by mechanical alloying. J Mater Process Technol 2003;139:434–9.
[29] Fadeeva VI, Leonov AV, Szewczak E, Matyja H. Structural defects and thermal stability of Ti(Al) solid solution obtained by mechanical alloying. Mater Sci Eng A 1998;242:230–4.
[30] Fan RH, Liu B, Zhang J, Bi J, Yin Y. Kinetic evaluation of combustion synthesis $3TiO_2 + 7Al = 3AlTi + 2Al_2O_3$ using nano-isothermal DSC method. Mater Chem Phys 2005;91:140–5.
[31] Murray JL. ASM handbook: alloy phase diagrams. ASM 1992;3:226–90.
[32] Dutkiewicz J, Maziarz W, Jaworska L. Structure of nanocrystalline Ti-based alloys obtained by mechanical alloying and ultra high pressure sintering. Rev Adv Sci 2008;18:264–8.
[33] Jakubowicz J, Adamek G. Preparation and properties of mechanically alloyed and electrochemically etched porous Ti6Al4V. Electrochem Commun 2009;11:1772–5.
[34] Warren BE. X-ray studies of deformed metals. Prog Metall Phys 1959;8:147–202.
[35] Enayati MH, Schamacher P, Cantor B. The structure and thermal stability of mechanically alloyed Ni–Nb–Zn amorphous alloys. J Mater Sci 2002;37:5255–9.
[36] Magdalena M. Kinetic behavior of titanium alloys Ti6Al4V and Ti6Al5Zr0.5Mo0.25Si in air and oxygen at a temperature range of 400–600 °C. Summary report; 1998.
[37] Sun F, Rojas P, Zuniga Z, Lavernia EJ. Nanostructure in a Ti alloy processed using a cryomilling technique. Mater Sci Eng A 2006;430:90–7.
[38] Niespodziana K, Jurczyk K, Jurczyk M. Titanium matrix nanocomposites fabricated by the mechanical alloying process. Mater Sci Poland 2008;26:341–8.
[39] Lu L, Lai MO. Mechanical alloying. New York: Kluwer Academic Publishers; 1998.
[40] Rocha SS, Adabo GL, Henriques GEP, Nobilo MAA. Vickers hardness of cast commercially pure titanium and Ti6Al4V alloy submitted to heat treatment. Braz Dent J 2006;17:126–9.
[41] Liu ZG, Bacarra B, Gabbitas B, Zhang DL. Production of Ti6Al4V based nanocomposites and their characterization. J Meta Nano Mater 2004;20/21:376–81.
[42] Mahboubi Soufiani A, Enayati MH, Karimzadeh F. Mechanical alloying behavior of Ti6Al4V residual scraps with addition of Al_2O_3 to produce nanostructured powder. J Mater Des 2010;31:3954–9.